

# SECOND-ORDER SEMI-IMPLICIT PARTITIONED METHOD FOR FLUID-STRUCTURE INTERACTION PROBLEMS

A. Naseri, I. Gonzalez, A. Amani and C. D. Pérez-Segarra

Heat and Mass Transfer Technological Center (CTTC)  
Universitat Politècnica de Catalunya - BarcelonaTech (UPC)  
ESEIAAT, C/ Colom 11, 08222 Terrassa (Barcelona), Spain  
e-mail: anaseri@cttc.upc.edu, web page: <http://www.cttc.upc.edu/>

**Key words:** Fluid-Structure Interaction, Partitioned Method, Semi-Implicit Coupling, Projection Method, Second-Order Temporal Accuracy

**Abstract.** This paper is concerned with numerical solution of fluid-structure interaction (FSI) problems involving an incompressible viscous flow and an elastic structure. A second-order time accurate semi-implicit method is proposed that separates the pressure term of the fluid equations and strongly couples it to the structure, while the rest of the fluid terms and the geometrical derivatives (moving mesh) are only loosely coupled. A second-order projection method is used to solve the fluid equations and also as a framework for the FSI coupling. Particular attention is paid to the accuracy of the fluid pressure in the projection method. The proposed coupling method retains the second-order accuracy for the coupled system. Numerical tests are carried out on a benchmark problem and the second-order accuracy for all the variables of interest (fluid velocity and pressure, and structural deformation) is demonstrated.

## 1 INTRODUCTION

Fluid-structure interaction (FSI) refers to problems with mutual interaction between a fluid flow and a moving or deforming structure. Fluid flow exerts surface forces on the structure which make it move or deform. The associated movement of the solid boundary, in return, alters the flow field. There are generally two approaches to solve the FSI problem, namely monolithic and partitioned. Monolithic methods solve the discrete fluid and structural equations simultaneously as a single system of equations, so the equilibrium condition on the interface is inherently observed. Partitioned methods, on the other hand, use separate solvers for fluid and structural sub-problems and adopt a coupling method to account for the interaction of the domains. Partitioned methods are broadly divided into loosely coupled (or explicit) and strongly coupled (or implicit) techniques. Loosely coupled methods solve the fluid and structural equations in sequence and only once per time step. These methods do not satisfy the exact equilibrium condition

on the interface which causes instability issues in FSI problems with low solid/fluid density ratios (so-called strong added-mass effect) [1, 2]. Implicit methods use coupling iterations between fluid and structural solvers to enforce the equilibrium condition on the interface. These methods are stable for problems with strong added-mass effect, however, their computational cost is normally very high due to the coupling iterations. To reduce the computational cost, Fernandez et al. [3] proposed a semi-implicit technique in which a fractional-step (projection) method is used for fluid equations and only the projection step is strongly coupled to the structure. This way the fluid pressure term and the structural deformation are strongly coupled while fluid convective and diffusive terms as well as the mesh movement step are left outside the coupling loop. Fluid pressure is the main contributor to the added-mass effect and coupling it explicitly would cause numerical instabilities in problems with low solid/fluid density ratios [1]. Thus, semi-implicit methods maintain the favorable stability of the implicit methods while reducing the computational cost. A similar method was proposed by Breuer et al [4] where the geometrical derivatives (dynamic mesh) are treated implicitly. Other very similar methods are presented in [5, 6]. An enhanced semi-implicit method was proposed by Naseri et al. [7, 8] where only the fluid pressure equation is strongly coupled to the structure. All the other fluid terms and the location of the interface are treated explicitly. The stability of the method was demonstrated for FSI problems with strong added-mass effect. It was shown that with a negligible loss of accuracy, this method could achieve much higher efficiency comparing to a fully implicit method [8]. The applicability of the method to FSI problems with turbulent flow was demonstrated in [9, 10].

Semi-implicit coupling techniques rely on a projection method to segregate the fluid pressure term. The pressure term is then coupled to the structure via coupling iterations. Thus, the projection method does not only serve to solve the fluid equations but also as a framework for the FSI coupling. The semi-implicit methods in [3, 4, 5, 8] have used a first order projection method for this purpose. Thus the overall temporal accuracy of these methods is one. He et al. [6] used a second-order pressure splitting scheme but no error analysis was presented to show that a second-order temporal accuracy was actually achieved. Extending a projection method to higher order temporal accuracy is not straightforward, as discussed in [11, 12, 13]. Although it is relatively easy to achieve second-order accuracy for velocity, fluid pressure remains only first-order accurate for many projection methods in the literature [11, 12, 13]. Considering that the fluid pressure is the main acting force on the structure, second-order accuracy for pressure is essential to achieve a second-order accurate FSI solution. Moreover, if the FSI coupling technique is not properly designed, the second-order accuracy for the coupled problem is not guaranteed, even though each sub-problem possessed such accuracy.

In this study, a second-order time accurate semi-implicit partitioned method for FSI problems with strong added-mass effect is proposed. A second-order projection method is used to solve the pressure-velocity coupling of the fluid equations and segregate the fluid pressure term. The fluid pressure is then strongly coupled to the structure. The proposed coupling method retains the second-order accuracy for the coupled FSI problem. Numerical tests are carried out on a benchmark test case and the second-order accuracy for

all the variables (fluid velocity and pressure, and structural deformation) is demonstrated.

## 2 GOVERNING EQUATIONS

In this section, the governing equations for each sub-problem domain and the coupling conditions on the interface are presented. The fluid and structural domains are referred to as  $\Omega_f(t)$  and  $\Omega_s(t)$  respectively, as they both vary in time. The interface of the domains is the shared boundary denoted by  $\Gamma(t) = \partial\Omega_f(t) \cap \partial\Omega_s(t)$ .

### 2.1 Fluid equations

The unsteady flow of an incompressible viscous fluid is governed by the Navier-Stokes equations. An Arbitrary Lagrangian-Eulerian (ALE) formulation of these equations in a moving domain is given by:

$$\frac{\partial \mathbf{u}}{\partial t} + \mathbf{c} \cdot \nabla \mathbf{u} = \frac{1}{\rho_f} \nabla \cdot \boldsymbol{\sigma}_f \quad (1)$$

$$\nabla \cdot \mathbf{u} = 0 \quad (2)$$

where  $\mathbf{u}$  is the fluid velocity and  $\rho_f$  the fluid density. Vector  $\mathbf{c}$  is the ALE convective velocity  $\mathbf{c} = \mathbf{u} - \mathbf{w}$ , which is the fluid velocity relative to a domain moving with a velocity  $\mathbf{w}$ . The stress tensor  $\boldsymbol{\sigma}_f$  is defined for a Newtonian fluid as:

$$\boldsymbol{\sigma}_f = -p\mathbf{I} + 2\mu_f\boldsymbol{\gamma} \quad (3)$$

where  $p$  is the fluid pressure,  $\mathbf{I}$  the unit tensor,  $\mu_f$  the dynamic viscosity of the fluid and  $\boldsymbol{\gamma}$  the strain rate tensor given by:

$$\boldsymbol{\gamma} = \frac{1}{2}(\nabla \mathbf{u} + \nabla \mathbf{u}^T) \quad (4)$$

### 2.2 Structural equations

The structural domain is governed by the nonlinear elastodynamics equation:

$$\rho_s \frac{D^2 \mathbf{d}}{Dt^2} = \nabla \cdot \boldsymbol{\sigma}_s \quad (5)$$

where  $\mathbf{d}$  stands for the structural position with respect to the reference configuration, and the structural density is shown by  $\rho_s$ . The Cauchy stress tensor  $\boldsymbol{\sigma}_s$  is related to the second Piola-Kirchhoff tensor  $\mathbf{S}_s$  by:

$$\mathbf{S}_s = J\mathbf{F}^{-1}\boldsymbol{\sigma}_s\mathbf{F}^T \quad (6)$$

where  $\mathbf{F}$  is the deformation gradient  $\mathbf{F} = \nabla \mathbf{d}$  and  $J$  is its determinant ( $J = \det(\mathbf{F})$ ).

The FSI method is presented for a general structure, however, for the test case in this paper the structure is considered to be an Euler-Bernoulli beam, governed by the following equation:

$$\rho_s A \frac{\partial^2 \mathbf{d}}{\partial t^2} + EI \frac{\partial^4 \mathbf{d}}{\partial x^4} = q(x, t) \quad (7)$$

where  $\mathbf{d} = [0, y, 0]^T$  in a Cartesian coordinate  $(x, y, z)$ ,  $A$  is the cross section area of the beam,  $I$  the second moment of area, and  $q$  is the normal load per unit length.

### 2.3 Coupling conditions

The coupling conditions apply at the interface  $\Gamma$  and account for the interaction of the domains. They are derived from the kinematic and dynamic equilibrium between the domains, which yield to the following conditions on a non-slip type interface:

$$\mathbf{u}_\Gamma = \frac{\partial \mathbf{d}_\Gamma}{\partial t} \quad (8)$$

$$\boldsymbol{\sigma}_s \cdot \mathbf{n}_\Gamma = \boldsymbol{\sigma}_f \cdot \mathbf{n}_\Gamma \quad (9)$$

for any point  $\mathbf{x} \in \Gamma$ , where  $\mathbf{n}_\Gamma$  is the unit normal vector on the interface. Equation (8) represents equality of the velocity of the fluid and the structure on the interface to assure the kinematic equilibrium. Equation (9) represents equality of the traction on the interface for dynamic equilibrium.

## 3 NUMERICAL METHOD

In this section we represent the time discretization of the governing equations and the FSI coupling method. It is assumed that the equations are semi-discretized in space using either a finite-volume or a finite-element method.

### 3.1 Fluid solver

A second-order time-discretized form of the Eq. (1) and (2) reads:

$$\frac{\mathbf{u}^{n+1} - \mathbf{u}^n}{\Delta t} = -(\mathbf{c} \cdot \nabla \mathbf{u})^{n+1/2} + \frac{\mu_f}{\rho_f} \nabla^2 \mathbf{u}^{n+1/2} - \frac{1}{\rho_f} \nabla p^{n+1/2} \quad (10)$$

$$\nabla \cdot \mathbf{u}^{n+1} = 0 \quad (11)$$

for any  $\mathbf{x} \in \Omega_f^{n+1}$ , and with a proper set of boundary conditions:

$$\begin{aligned} \mathbf{u}_\Gamma^{n+1} &= \frac{\partial \mathbf{d}_\Gamma^{n+1}}{\partial t} && \text{on } \Gamma^{n+1} \\ \mathbf{u}_{\partial_D}^{n+1} &= \mathbf{u}_b && \text{on } \partial_D \Omega_f^{n+1} \\ \frac{\partial \mathbf{u}_{\partial_N}^{n+1}}{\partial \mathbf{n}} &= 0 && \text{on } \partial_N \Omega_f^{n+1} \end{aligned} \quad (12)$$

where  $\partial_D$  and  $\partial_N$  represent, respectively, the Dirichlet and Neumann boundaries,  $\mathbf{n}$  is the normal direction and  $\mathbf{u}_b$  the assigned velocity on the boundary.

We use an incremental pressure-correction projection method, similar to [14, 15], to solve the momentum equation. Thus, an intermediate velocity is evaluated using the last known pressure field. Unlike the original projection method of Chorin [16], this method does not impose a formal first-order splitting error. We use an explicit Adams-Bashforth method for the convective term and a Crank-Nicolson method for the diffusive term. This choice of discretization schemes is by no means restrictive. Any second-order discretization is permitted. Therefore the intermediate velocity field is evaluated as:

$$\frac{\mathbf{u}^* - \mathbf{u}^n}{\Delta t} = -\left[\frac{3}{2}(\mathbf{c} \cdot \nabla \mathbf{u})^n - \frac{1}{2}(\mathbf{c} \cdot \nabla \mathbf{u})^{n-1}\right] + \frac{\mu_f}{2\rho_f}(\nabla^2 \mathbf{u}^* + \nabla^2 \mathbf{u}^n) - \frac{1}{\rho_f} \nabla p^{n-1/2} \quad (13)$$

The same set of boundary conditions as in Eq. (12) is used for the intermediate velocity. This velocity field is then projected onto a space of divergence-free vector fields:

$$\mathbf{u}^* = \mathbf{u}^{n+1} + \frac{\Delta t}{\rho_f} \nabla \phi^{n+1} \quad (14)$$

$$\nabla \cdot \mathbf{u}^{n+1} = 0 \quad (15)$$

where  $\phi^{n+1}$  is a scalar field obtained by:

$$\nabla^2 \phi^{n+1} = \frac{\rho_f}{\Delta t} \nabla \cdot \mathbf{u}^* \quad (16)$$

$$\mathbf{n} \cdot \nabla \phi^{n+1}|_{\partial\Omega_f} = 0 \quad (17)$$

Substituting Eq. (14) into Eq. (13) and comparing it to Eq. (10), the equation to recover the fluid pressure is obtained:

$$p^{n+1/2} = p^{n-1/2} + \phi^{n+1} - \frac{\mu_f \Delta t}{2\rho_f} \nabla^2 \phi^{n+1} \quad (18)$$

The second term in the pressure recovery equation is essential to retain the second-order accuracy for pressure up to the boundary. Without this term the Neumann boundary condition for the scalar field  $\phi$  transmits to the pressure itself and imposes an artificial, numerical boundary layer [12]. Pressure at the new time station  $t^{n+1}$  could be evaluated by a second-order extrapolation from half-time levels:

$$p^{n+1} = \frac{3}{2}p^{n+1/2} - \frac{1}{2}p^{n-1/2} \quad (19)$$

Pressure at  $t^{n+1}$  is not used in the discretized fluid equations but it is needed to evaluate the fluid force on the structure at the new time step. A common inaccuracy in some articles in the literature is omitting this extrapolation and evaluating  $p^{n+1}$  by Eq. (18). However, this is not consistent with the mid-point discretization at Eq. (10). If the pressure at Eq. (18) were considered to be at time  $t^{n+1}$  instead of  $t^{n+1/2}$ , it will always carry a first-order error due to the time lag.

### 3.2 Dynamic mesh

As the solid boundary is deformable, fluid mesh needs to move to adapt to the new location of the interface and the discrete domain velocity on the mesh surfaces  $\mathbf{w}^{n+1}$  needs to be evaluated. A parallel moving mesh technique, based on radial basis function interpolation method [17], is used to move the fluid grid in accordance to the new location of the interface. Surface velocities are evaluated according to the so-called space conservation law which guarantees no volume is lost while moving the grid. Detailed description of the dynamic mesh method could be found in [17, 8]. Here we will use the function  $\mathcal{M}$  to refer to the mesh movement step:

$$(\Omega_f^{n+1}, \mathbf{w}^{n+1}) = \mathcal{M}(\mathbf{d}_\Gamma^{n+1}) \quad (20)$$

### 3.3 Structural solver

Structural equations are discretized in time using a second-order Newmark method. Defining the structural velocity  $\mathbf{v} = \frac{\partial \mathbf{d}}{\partial t}$ , the semi-discretized structural equation reads:

$$\mathbf{v}^{n+1} = \mathbf{v}^n + \frac{\Delta t}{2\rho_s A} [(q^{n+1} - EI \frac{\partial^4 \mathbf{d}}{\partial x^4})^{n+1} + (q^n - EI \frac{\partial^4 \mathbf{d}}{\partial x^4})^n] \quad (21)$$

and the new location of the structure could be calculated as:

$$\mathbf{d}^{n+1} = \mathbf{d}^n + \frac{\Delta t}{2}(\mathbf{v}^{n+1} + \mathbf{v}^n) \quad (22)$$

It should be noted that using a simplified structural model is not restrictive for the proposed FSI coupling method, since it is used as a black-box module. Any structural solver with a second order temporal accuracy could be used. We will use the notation  $\mathcal{S}$  to refer to the structural solver as a function of surface stress on the interface:

$$\mathbf{d}_\Gamma = \mathcal{S}(\boldsymbol{\sigma}_\Gamma) \quad (23)$$

where  $\mathbf{d}_\Gamma$  is the location of the interface and  $\boldsymbol{\sigma}_\Gamma$  is the stress on the interface exerted by the fluid  $\boldsymbol{\sigma}_\Gamma = \boldsymbol{\sigma}_f(p, \mathbf{u})_\Gamma \cdot \mathbf{n}_\Gamma$ .

### 3.4 Coupling method

We present a semi-implicit FSI coupling method in which only the fluid pressure term is strongly coupled to the structure via coupling iterations. The remaining fluid terms as well as the dynamic mesh step are evaluated only once per time step. The complete FSI solution method from  $t^n$  to  $t^{n+1}$  is as follows.

Semi-implicit FSI coupling method:

**step 0:** extrapolation of  $\mathbf{d}_\Gamma$  from previous time steps:

$$\tilde{\mathbf{d}}_\Gamma^{n+1} = 2.5\mathbf{d}_\Gamma^n - 2\mathbf{d}_\Gamma^{n-1} + 0.5\mathbf{d}_\Gamma^{n-2} \quad (24)$$

**step 1:** moving the fluid mesh (*explicitly coupled*):

$$(\Omega_f^{n+1}, \mathbf{w}^{n+1}) = \mathcal{M}(\tilde{\mathbf{d}}_\Gamma^{n+1}) \quad (25)$$

**step 2:** ALE convection-diffusion equation (*explicitly coupled*):

$$\begin{aligned} \frac{\mathbf{u}^* - \mathbf{u}^n}{\Delta t} &= -\left[\frac{3}{2}(\mathbf{c} \cdot \nabla \mathbf{u})^n - \frac{1}{2}(\mathbf{c} \cdot \nabla \mathbf{u})^{n-1}\right] \\ &+ \frac{\mu_f}{2\rho_f}(\nabla^2 \mathbf{u}^* + \nabla^2 \mathbf{u}^n) - \frac{1}{\rho_f} \nabla p^{n-1/2} \quad \text{in } \Omega_f^{n+1} \end{aligned} \quad (26)$$

**step 3:** pressure equation and structural solver (*implicitly coupled, solved iteratively*):

$$\mathbf{u}_\Gamma^* = \frac{3\mathbf{d}_\Gamma^{n+1} - 4\mathbf{d}_\Gamma^n + \mathbf{d}_\Gamma^{n-1}}{2\Delta t} \quad \text{on } \Gamma^{n+1} \quad (27)$$

$$\nabla^2 \phi^{n+1} = \frac{\rho_f}{\Delta t} \nabla \cdot \mathbf{u}^* \quad \text{in } \Omega_f^{n+1} \quad (28)$$

$$p^{n+1/2} = p^{n-1/2} + \phi^{n+1} - \frac{\mu_f \Delta t}{2\rho_f} \nabla^2 \phi^{n+1} \quad \text{in } \Omega_f^{n+1} \quad (29)$$

$$p^{n+1} = \frac{3}{2}p^{n+1/2} - \frac{1}{2}p^{n-1/2} \quad \text{in } \Omega_f^{n+1} \quad (30)$$

$$\boldsymbol{\sigma}_\Gamma^{n+1} = \boldsymbol{\sigma}_f(p^{n+1}, \mathbf{u}^*)_\Gamma \cdot \mathbf{n}_\Gamma \quad \text{on } \Gamma^{n+1} \quad (31)$$

$$\mathbf{d}_\Gamma^{n+1} = \mathcal{S}(\boldsymbol{\sigma}_\Gamma^{n+1}) \quad \text{on } \Gamma^{n+1} \quad (32)$$

**step 4:** velocity correction (*explicitly coupled*):

$$\mathbf{u}^{n+1} = \mathbf{u}^* - \frac{\Delta t}{\rho_f} \nabla \phi^{n+1} \quad \text{in } \Omega_f^{n+1} \quad (33)$$

$$\mathbf{u}_\Gamma^{n+1} = \frac{3\mathbf{d}_\Gamma^{n+1} - 4\mathbf{d}_\Gamma^n + \mathbf{d}_\Gamma^{n-1}}{2\Delta t} \quad \text{on } \Gamma^{n+1} \quad (34)$$

Step 3 of the above algorithm is where fluid pressure is strongly coupled to the structure. This step provides for the stability of the method for FSI problems with strong added-mass effect. Loose coupling of the remaining steps significantly reduces the computational cost of the simulations. A Newton-Krylov method with approximated Jacobian [7] is used to carry out the coupling iterations in step 3.

## 4 NUMERICAL TESTS

Numerical tests are carried out on a benchmark problem studied in [2, 18], among others. The test case is a 2-D lid-driven cavity of a  $1m \times 1m$  with a flexible bottom. The top boundary of the cavity is moving with an oscillatory speed of  $u(t) = 1 - \cos(\omega t)$  with  $\omega = 2\pi/5$ . There are two openings of  $0.1m$  length on the sidewalls that allow the fluid to enter to and exit from the domain. Figure 1(left) shows a schematic description of the problem. The fluid density and viscosity are  $\rho_f = 1.0kg/m^3$  and  $\mu_f = 0.01Pa.s$ , respectively. The flexible structure at the bottom has a thickness of  $h = 0.05m$ , the structural density is  $\rho_s = 5kg/m^3$  and the Young modulus  $E = 250N/m^2$ .

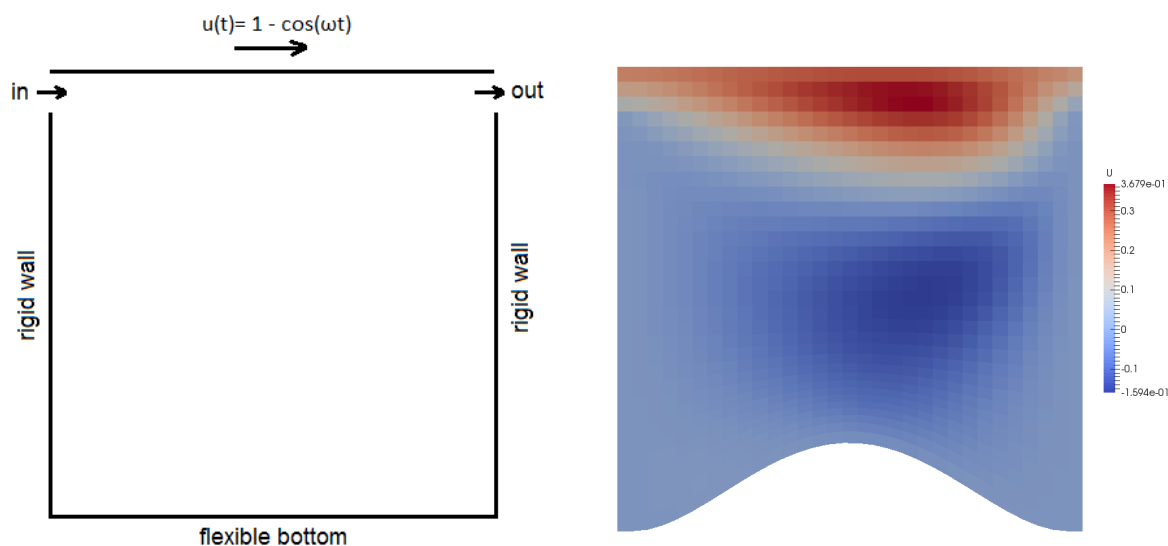


**Figure 1:** Driven cavity with flexible bottom, Left: schematic view of the problem setup, Right: flow field inside the deformed domain at  $t = 9s$ .

The flexible bottom is modeled as an Euler-Bernoulli beam, as mentioned earlier. A classical  $31 \times 31$  spatial grid is used to solve the problem. Spatial discretization is carried out using a finite volume method with second-order central difference schemes. The structure is a thin membrane so the fluid mesh elements on the interface are also used as the computational grid for the structural equations. Thus, the structural grid nodes match the fluid mesh on the interface and there is no need for interpolation of parameters between the domains. Figure 1(right) shows the flow field inside the domain with structural deformation at the bottom, at  $t = 9s$  (near maximum deflection).

To evaluate the temporal accuracy of the method, the problem is solved using four different time step sizes ranging from  $5 \times 10^{-4}$  to  $4 \times 10^{-3}s$ . In the lieu of an exact solution, reference results are obtained using a much smaller time step of  $\Delta t = 1 \times 10^{-4}s$ . The spatial grid is kept constant for the tests. The simulations are carried out from  $t = 0s$  until  $t = 1s$ , when the results for different time steps are saved and compared to the reference solution. The error is evaluated at every grid node and presented in both  $L_2$  and  $L_\infty$  norms.

Figures 2 and 3 represent the variation of the absolute error with time step size  $\Delta t$  in logarithmic scales. Figure 2 represents the error of fluid velocity and pressure inside the fluid domain, while Figure 3 represents the error of fluid pressure and structural deformation on the fluid-structure interface. Results demonstrate a clear second-order temporal accuracy for all the variables of interest in both  $L_2$  and  $L_\infty$  norms.

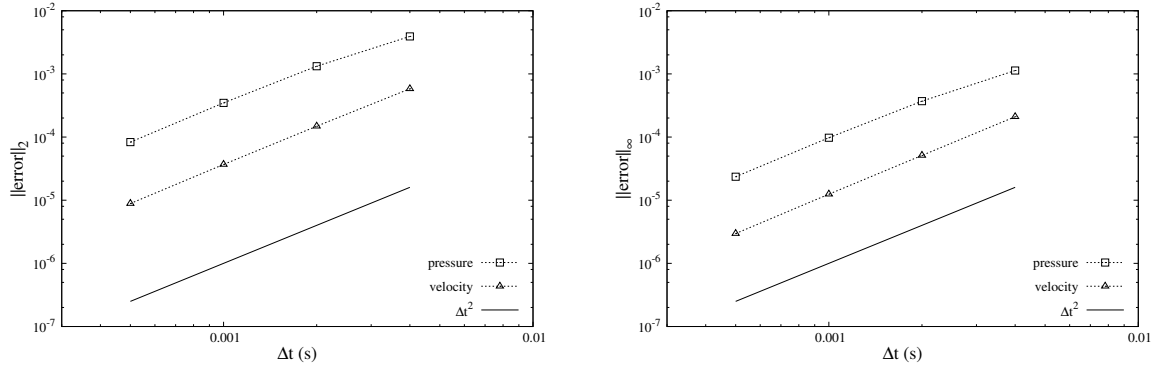


**Figure 2:** Variation of absolute error inside the fluid domain by time step size, Left:  $L_2$  norm, Right:  $L_\infty$  norm.

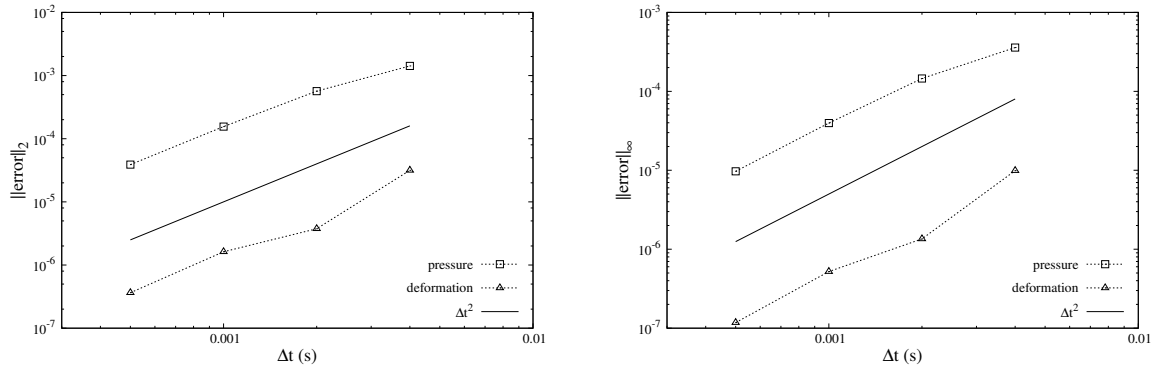


**Figure 3:** Variation of absolute error on the fluid-structure interface by time step size, Left:  $L_2$  norm, Right:  $L_\infty$  norm.

## 5 CONCLUSIONS

A second-order semi-implicit method for partitioned solution of fluid-structure interaction problems is proposed. The method uses a second-order projection method to solve the fluid equations and also as a framework for the FSI coupling. The fluid pressure term is effectively segregated using the projection method and is strongly coupled to the structure via Newton iterations. The remaining fluid terms and the geometrical nonlinearities (moving mesh) are treated explicitly and thus evaluated only once per time step. Second-order accuracy of the method for a coupled FSI problem is numerically demonstrated.

## 6 Acknowledgement

This work was partially funded by the Ministerio de Economía y Competitividad, Secretaría de Estado de Investigación, Desarrollo e Innovación, Spain (ENE2017-88697-R), and a FI PhD scholarship by the Agència de Gestió d'Ajuts Universitaris i de Recerca (AGAUR) of Generalitat de Catalunya.

## REFERENCES

- [1] P. Causin, J. F. Gerbeau, and F. Nobile. *Comput. Methods Appl. Mech. Eng.*, 194:4506–4527, 2005.
- [2] C. Förster, W. A. Wall, and E. Ramm. *Comput. Methods Appl. Mech. Eng.*, 196:1278–1293, 2007.
- [3] M. A. Fernández, J-F Gerbeau, and C. Grandmont. *Int. J. for Numer. Methods Eng.*, 69(4):794–821, 2007.
- [4] M. Breuer, G. De Nayer, M. Münsch, T. Gallinger, and R. Wüchner. *J. Fluids Struct.*, 29:107–130, 2012.
- [5] M. Astorino, F. Chouly, and M. A. Fernández. *SIAM J. on Sci. Comput.*, 31(6):4041–4065, 2009.
- [6] T. He, K. Zhang, and T. Wang. *Commun. Comput. Phys.*, 21(5):1449–1474, 2017.
- [7] A. Naseri, O. Lehmkuhl, I. Gonzalez, and A. Oliva. *J. Phys. Conf. Ser.*, 745(3):032020, 2016.
- [8] A. Naseri, O. Lehmkuhl, I. Gonzalez, E. Bartrons, C. D. Pérez-Segarra, and A. Oliva. *J. Fluids Struct.*, 80:94–112, 2018.
- [9] I González, O Lehmkuhl, A Naseri, J Rigola, and A Oliva. In *International Compressor Engineering Conference*, page 2490. Purdue University Libraries, 2016.
- [10] I. González, A. Naseri, J. Rigola, C. D. Pérez-Segarra, and A. Oliva. *IOP Conf. Ser. Mater. Sci. Eng.*, 232(1):012032, 2017.
- [11] J. L. Guermond, P. Minev, and J. Shen. *Comput. Methods Appl. Mech. Eng.*, 195(44-47):6011–6045, 2006.
- [12] D. L. Brown, R. Cortez, and M. L. Minion. *J. Comput. Phys.*, 168(2):464–499, 2001.
- [13] S. Armfield and R. Street. *Int. J. for Numer. Methods Fluids*, 38(3):255–282, 2002.
- [14] J. Van Kan. *SIAM J. on Sci. Stat. Comput.*, 7(3):870–891, 1986.
- [15] J. B. Bell, P. Colella, and H. M. Glaz. *J. Comput. Phys.*, 85(2):257–283, 1989.

- [16] A. J. Chorin. *Math. Comput.*, 22:745–762, 1968.
- [17] O. Estruch, O. Lehmkuhl, R. Borrell, C. D Pérez Segarra, and A. Oliva. *Comput. Fluids*, 80:44–54, 2013.
- [18] U. Küttler and W. A. Wall. *Comput. Mech.*, 43:61–72, 2008.